Fully printed, stretchable and wearable bioimpedance sensor on textiles for tomography

Peer-reviewed author version

JOSE, Manoj; LEMMENS, Marijn; BORMANS, Seppe; THOELEN, Ronald & DEFERME, Wim (2021) Fully printed, stretchable and wearable bioimpedance sensor on textiles for tomography. In: FLEXIBLE AND PRINTED ELECTRONICS, 6 (1) (Art N° 015010).

DOI: 10.1088/2058-8585/abe51b
Handle: http://hdl.handle.net/1942/33896

Fully Printed, Stretchable and Wearable Bioimpedance Sensor on Textiles for Tomography

Manoj Jose[1,2], Marijn Lemmens[1,2], Seppe Bormans[1,2], Ronald Thoelen[1,2], and Wim Deferme[1,2]

[1] Hasselt University, Institute for Materials Research (IMO-IMOMEC) 1, 3590 Diepenbeek, Belgium
[2] IMEC vzw – Division IMOMEC, Wetenschapspark 1, B-3590 Diepenbeek, Belgium
E-mail: wim.deferme@uhasselt.be

Received xxxxxx
Accepted for publication xxxxxx
Published xxxxxx

Abstract

Electrical impedance tomography (EIT) is a non-invasive, real-time, continuous imaging technique that has multiple applications in health care. EIT is a realizable technique for radiation-free medical imaging ranging from real-time monitoring of bone fracture repair to lung functioning. This work explores the prospect of printing a wearable bioimpedance sensor on textiles for EIT imaging. Screen printing and Stencil printing were applied to fabricate the sensor on the textile substrate and the imaging was carried out with the worn sensor on the human body. The first part of the work focuses on developing a flexible textile sensor in the form of a bracelet to obtain cross-sectional images of the forearm that unravel bone features like shape, size and position. However, body parts such as the thorax have added complexities due to their constantly varying perimeter and uneven shape. It is a significant prerequisite for the wearable sensors to apply to dynamic body parts where irregular shape and continuous volume variations occur. The second part of the article therefore addresses the fabrication and testing of a stretchable textile-based sensor to address such instances of body dynamicity. The proposed stretchable sensor, worn on the thorax, demonstrates the feasibility of imaging such an uneven and dynamic body part. Although the EIT images are inherently attributed to low resolution, this work shows the prospect of wearable imaging applications in health monitoring. Apart from demonstrating the printed sensor for EIT imaging, the article shows the image rendering quality dependency over the frequency of the signal and the number of electrodes. This work could light up to initiate further research on wearable EIT based health monitoring devices for real-life scenarios.

Keywords: Bioimpedance sensor, EIT, Printing, wearable, Textile, Tomography

1. Introduction

The importance of personal health care systems for non-invasive health assessment and disease diagnosis has grown in recent years [1]. After the introduction of flexible electronics into bio-medical applications, demand for wearable and portable devices ascended. Also, the application of advanced communication technologies resulted in a paradigm shift from a hospital centred health care model to a preventive and personal health care model [2-4]. Modern wearable health monitoring systems demand for certain prerequisites like the compatibility to continuous monitoring in a non-invasive way and the ease of use. Along with the functionality requirements, the wearable device has to be deformable, conformable, economical and preferably fabricated on textiles, also known as smart textiles [5, 6].

With the rising market for wearable electronics, the smart textile concepts also grabbed attention and started to grow [5, 7]. Smart textile production has got several roots from weaving, embroidering, knitting and printing techniques ultimately producing various devices, from the temperature, strain and Electrocardiogram (ECG) sensors to light-emitting, energy harvesting and logic circuit devices [8-11]. Among the different production techniques, printing seems to be more attractive as it offers the freedom to deposit a wide range of material compositions (silver, carbon, piezoelectric, dielectric, semiconducting polymer inks) to produce flexible and soft functional textiles at a higher speed and a lower cost [12-14]. Proper designing of the sensor architecture and the selection of suitable inks makes the wearable device bio-compatible for the human body.

Printing of conductive structures on fabric has already been reported in the literature and screen printing is an obvious choice for fabric printing since it is known for thick (even above 10µm) material deposition [14, 15]. Typically roughness and absorption are the two main constraints for printing on the textile substrates. To acquire adequate uniformity and wettability for the surface over which conductive electrodes are printed, Gordon et al. reported of coating a planarizing layer of polyurethane on the textile and applied the sensor for biopotential measurements [16]. Hong et al. developed a textile-based wearable compact sensor system for EIT imaging of breast cancer. The electrodes are fabricated on textiles applying planar fashionable circuit board technology (P-FCB) and tested on phantom made up of agar and carrot for breast and cancer tissues, respectively. This study shows that cancer tissues of even 5mm in size could be detected with their EIT sensor [17]. Researchers from UC Berkeley presented their investigations about printing a bioimpedance tomographic sensor on foil for pressure ulcer detection. The findings were quite encouraging and showed ulcer formation over time by applying constant pressure and ulcer detection with a corresponding decrease in the impedance of the mice tissues [18].

EIT imaging is based on the mapping of bioimpedance distribution, measuring the electrical response of the biological body to applied electrical signals. This work discusses the EIT imaging of the human body which comprises of different tissues. Each kind of tissue has unique electrical properties that depend on its composition. Tissues consist of cells, and the cells are mainly built up of cell membrane and aqueous contents. A living cell possesses a capacitive nature with an ion-rich conductive cytoplasm embedded in a conductive extracellular fluid separated by a constant phase element cell membrane. Cell membranes mainly consist of lipid layers and proteins are attached to it. Their proportion varies with the tissue types in which the lipids are mainly made up of glycerol and fatty acids. In contrast, the building unit of protein is amino acids. The polarity of these molecules is pertinent in determining the dielectric properties of the cell membrane.

Along with this, the aqueous part also plays a role in the properties of the tissue. For comparison, the bone marrows water content is 8-16%, whereas it is 73-78% in muscle tissues. The conductivity of the tissues is majorly due to the presence of ions. In an electric field, the conduction current in the tissue mainly depends on ion mobility and its concentration. The bound charges within tissues such as polar molecules and electrical double layers contribute to their complex dielectric properties [19]. The characteristic changes of the electrical signals, while passing through a biological medium according to the impedance changes, account for the bioimpedance measurements. These measurements also depend on the applied signal frequency. The low-frequency signals would prefer an irregular passage through the extracellular fluid having a lower impedance, while the high-frequency signals would travel relatively straight across the cell membrane as shown in Fig.1 [20-23].

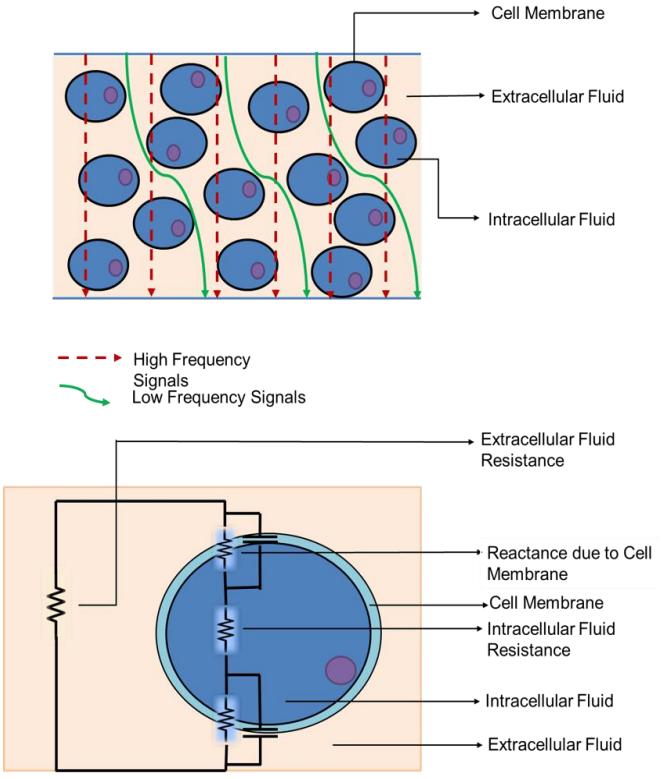

Fig.1 Depiction of low frequency and high-frequency current signal behavior in living tissues (upper image). Equivalent circuit diagram of current passing through tissue (lower image) [24].

Electrical impedance-based body analysis, imaging and diagnosis are embedded in health care practices and there are many applications developed based on impedance measurements of the body [21, 24-27]. EIT enables to draw the conductivity map (2D or 3D image) of the specimen to reveal the physiology, composition and damages of the region

of interest [22]. The device consists of an array of electrodes arranged around the test specimen. When a small alternating current is applied between two electrodes, the corresponding potential difference generated is measured at all other electrode pairs. Bioimpedance based tomography can be a miniature application of medical imaging techniques and finds applications as wearable and portable health monitoring systems. As a wearable functionality, it can be a promising technique for continuous monitoring of wound healing, pulmonary functioning, fracture monitoring, stroke detection and many more reported in the past [18, 24, 28, 29]. EIT could guide the ventilator settings for a mechanically ventilated patient and such systems are commercially available [28, 30, 31]. All the mentioned health monitoring applications explicitly demand a non-radiative, low cost, portable and wearable device for continuous imaging, where computed tomography (CT) or magnetic resonance imaging (MRI) becomes impractical. It is a fact that EIT imaging doesn't provide high spatial resolution images as above mentioned techniques, however high temporal resolution of the EIT images is a prerequisite in many biomedical applications [24].

The first EIT image was produced decades before and the technique lodged immense growth prospects. Nevertheless, it had a low-paced development towards commercialization and it is less adapted for real-life applications [30]. Medical electrodes with their associated circuitries are being used for EIT imaging over these years. Inconvenience caused by three-dimensional metal structures, and cumbersome and limited portability restricted the medical electrodes from continuous monitoring applications. In addition to this, the difficulties arising from the equidistant electrode placement and the pain caused by the adhesives on removing the electrodes makes them less attractive. This article provides a feasibility study leading towards a new category of devices that can meet the functional requirements of wearability and EIT imaging in textile platforms for health monitoring.

This study's main focus lies in the fabrication of two dimensional EIT sensors on textile substrates, applying different printing techniques. The smart selection of materials and appropriate printing processes ensures the flexibility and/or stretchability of the sensor on textiles at low production costs. The electrodes printed at equidistance in the textile sensor and its soft interface with the skin provide comfortability and reduce the practical difficulties in the medical electrodes' attachment. The initial part of the article discusses the fabrication of a textile-based (flexible but not stretchable) sensor in the form of a bracelet for EIT imaging of the forearm cross-section. The latter part deals with relatively more complex thorax imaging that is challenged from continuous volume changes due to breathing. This section also tries to address the problems like proper sensor-skin contact and comfort in wearability through a stretchable textile sensor. In contrast to the sensor fabrication for static body part imaging, distinct sensor fabrication strategies are adopted with an appropriate substrate and material selection for the imaging of dynamic human body segments. Heading towards a proof-of-concept device, the sensor effectivity is tested for human forearm and thorax imaging respectively.

2. MATERIALS AND METHODS

2.1 Materials and processing for sensor fabrication

The proposed work applies textile substrates for sensor fabrication, as they are considered one of the most convenient wearable platforms. Non-stretchable and stretchable textiles with the modulus of elasticity of 48 MPa and 0.188 MPa respectively are used in the work (up to 25% of stretching). The fabrication starts with electrode printing and silver is an excellent choice as an electrode material due to its high stability, low-temperature processability and cost-effectiveness. Above all, it is used in wearables due to the low contact impedance offered as it is redox-active; meanwhile, its relatively short lifetime compared to gold and platinum is a major downside. A silicone elastomer is deployed as one of the top layers to supplement the conductive tracks' insulation and serve as biocompatible skin contact. Furthermore, it helps to omit the relative movements (slip) of the worn sensor as its mechanical properties are analogous to the skin[32]. This could help to avoid the motion artefacts and better EIT imaging of the human body. However, there are constraints in the printing of textile sensors. The substrate's roughness and high ink absorption nature are challenging to turn it to functional with printing and coating. To address such issues, thick film deposition techniques such as screen printing, stencil printing and blade coating are used to deposit the different functional materials.

Screen printing is a conventional technique categorized as a thick film material deposition method [33]. The setup comprises a fabric screen stretched and attached to a frame, where the unwanted areas of the screen are masked with a suitable emulsion. The thickness of the emulsion coating is the prime factor deciding the thickness of the printed layer [34]. The functional material in the form of printing ink is pushed through the unmasked areas of the screen with the help of a rubber squeegee onto the substrate. Screen printing is widely used for textile printing applications and in recent times, it is found adapted into smart textiles as well. Screen printing is applied in this work because of its excellent attribute to print on textiles [35]. This work used ISIMAT P1000, an automatic screen printing machine from Germany to print silver and insulative material inks. The screen fabric was made up of polyester with 140 threads/cm and a thread diameter of 31 µm is used for the screen preparation (As per the sensor design, the screen printing screens are prepared at Mekascreen, Brussels).

Blade coating is a relatively simple technique to deposit a wide range of material compositions. Here the blade and substrate gap can be controlled with micrometer gauges on the top side of the blade. Blade coating is mainly used in this work to deposit a uniform layer of silicone elastomer. It is made with a coating instrument from MTI Corporation, USA (Model MSK-AFA-II-220). The coating instrument is capable of making wet films thickness ranging from 5 to 3000 µm. The gap between the blade and substrate is approximated to 200 µm for the silicone elastomer coating. The stencil printing technique is considered in the same category of screen printing but as an older format of it [34]. In this work, a mask (stencil) is designed using Adobe Illustrator software, later transferred to a masking substrate. The masks are realised on a polymer foil where the areas of material deposition are left open. This is made possible with the use of a laser engraver (Trotec, speedy R100 CO2 laser) to selectively remove the masking sheet. The masking sheet is a thermoplastic polyurethane (TPU) foil (from Grafytip, Belgium) with liner sheet support. After the laser removal of the mask opening areas, the liner is removed and placed on the textile substrate. As the TPU foil is mildly adhesive to the textiles, the squeegee does not let the mask move from its position during printing. The printing paste is pushed through the mask openings and the wet film thickness would be approximately equal to the thickness of the masking sheet. This way, one could obtain a higher aspect ratio and thicker ink deposition with patterning prospects.

2.2 Fabrication of the flexible textile sensor

The textile substrate used for this sensor is a polyester woven fabric (100% polyester - washed and fixated - kw11401) from Concordia Textiles (Valmontheim, Belgium) with an average roughness of 6µm. It has shown good printability and flexibility properties and is stable up to 140°C. The conductive ink, Flexible silver paste (C2131121D3) of sheet resistance 100mΩ/Square, viscosity 6.5 - 8.5 Pa.s) and the insulating ink (D2090130P4) were purchased from Gwent group (Pontypool, United Kingdom) which has already proved for its flawless performance for the flexible device applications [14]. A silicone elastomer, Polydimethylsiloxane (PDMS) Sylgard 184 (base A) and curing agent (base B) were purchased from Dow Corning Corporation.

The substrate was first processed at 120 °C for 10 minutes to avoid dimensional stability problems during the printing and curing. Subsequently, a predesigned electrode structure was applied to the fabric using screen printing (roll-to-roll process compatible technique) with the flexible silver paste. The printed structure was kept in a box oven at 120 °C for 10 minutes to remove the solvent part of the deposited ink and further sinter the ink to make the structures conductive. As a next step, a layer of insulating paste was screen printed over the silver tracks. Only the conductive tracks were covered while the electrodes for skin-contact were kept uncovered. The insulation layer was cured at 120 °C and a layer thickness of 10-15µm was achieved. Then an additional layer of PDMS was deposited over the insulation layer. The PDMS base A and base B (curing agent) were mixed in the weight ratio 10:1 and this mixture was deposited using a blade coating applicator. To avoid the PDMS inflow into the electrode area, those are masked with a paper tape. The resulted PDMS film was cured at 70°C in a box oven for 1 hour. As a final step, electrode gel (Signa electrode gel from Parker Laboratories, New Jersey, USA) was stencil printed over the electrodes.

2.3 Fabrication of the stretchable textile sensor

A stretchable sensor was designed on top of an elastic polyester textile substrate (from Concordia Textiles Valmontheim, Belgium) of length 70 cm and 16 electrodes were arranged at equidistance. Unlike the substrate used for the non-stretchable (flexible) sensor, the one used here is rough and more absorptive which does not let screen printing be the deposition technique of choice. Therefore, stencil printing was used to deposit thick layers of silver paste PE873, Dupont (stretchable conductor) through a mask for realizing the electrodes and the tracks (Fig.2). Selectively removed electrode areas in the mask help to carry out thick layer deposition of silver paste followed by its curing step at 110°C in a box oven for 20 minutes. Subsequently, an insulating ink Tubicoat Mea from CHT group (polyurethane-based and compatible with stretching) was printed through another mask to ensure that the tracks are not causing any interference when touching the body. Thanks to this selective deposition method, the textile well maintained its stretchability. The sensor fabrication underwent the deposition of a thin, uniform layer of PDMS and it was cured as mentioned previously. During this step, the electrode area was kept masked to avoid PDMS deposition on skin-contacting areas of the electrode. As a final fabrication process, an electrode gel is deposited on the

electrode's skin-contacting areas as mentioned in the previous section.

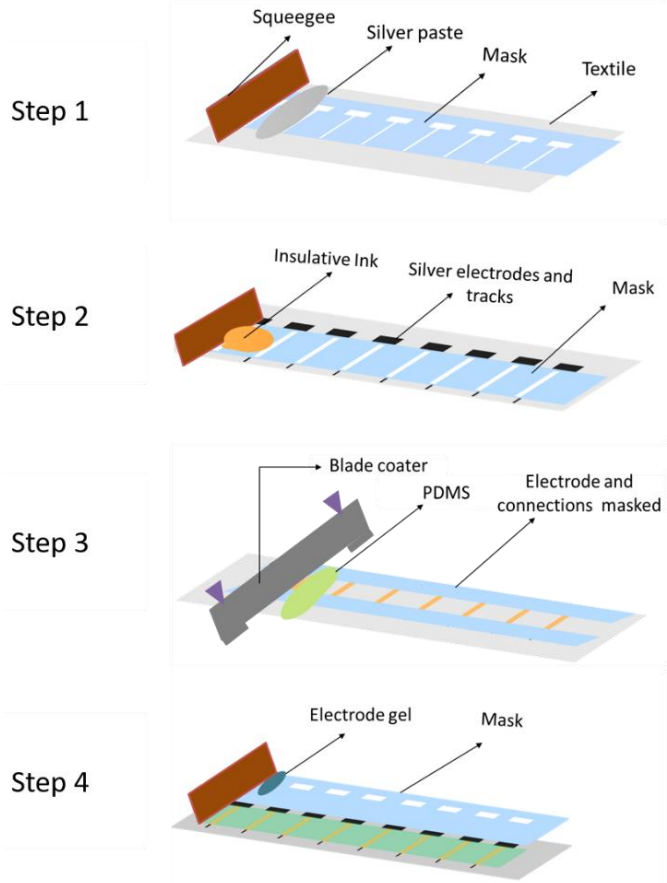

Fig.2 Stretchable sensor preparation. Step1: printing Silver paste on stretchable textiles, Step 2: printing insulative ink on tracks (leaving out the electrode and connection ends), step 3: blade coating PDMS, step 4: electrode gel deposition

2.4 Measurement Methodology

EIT image reconstruction is a technique that gives the possibility to reconstruct the electrical conductivity distribution of a closed domain in a conductive medium based on the surface potential generated at the boundaries on injecting a known current signal. To do this, different measurement patterns available were studied [36].

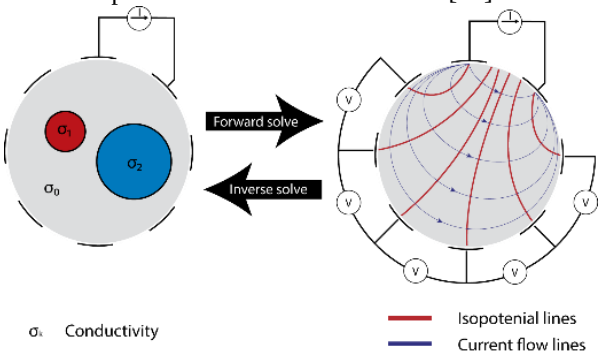

Fig.3 Measurement methodology overview

EIT, similar to other soft tomography techniques, defines diffusive probing energy which results in a significant variation of sensitivity in the domain of interest. Reconstruction of such images requires an inverse problem technique. A nonlinear method is used to solve this problem, the Gauss-Newton solver [37]. It solves the inverse problem by iterative linearization of the nonlinear relationship between the impedance and the electrical potential measurements. To do this, the Jacobian (sensitivity) matrix is recalculated for each iteration allowing the finding of the minimal error between the measured value and calculated value.

$$s = \frac{1}{2}\,(V_m - V_c)^T\,(V_m - V_c) \qquad \text{(Eq. 1)}$$

With s standing for a function describing the conductivity at a specific point, V_m is the measured potential value at the boundary and V_c the calculated potential value. This algorithm provides a reconstruction image of the conductivity distribution. However, as previously mentioned, the ill-posed inversion problem in EIT must be regularized.

$$\min_{\sigma}\left\{\frac{1}{2}\|V_m - f\|^2 + \lambda\|G(\sigma)\|^2\right\} \qquad \text{(Eq. 2)}$$

Equation (2) describes a general framework of EIT, here the term $(G(\sigma))$ represents a matrix for the regularization term. Based on this equation the conductivity matrix of an unknown domain can be calculated showing the inconsistencies regarding the conductivity distributions at each point in the predefined finite element model.

2.5 Measurement Pattern

In theory, a four-point configuration provides a more accurate impedance measurement than a two-point configuration because the parasitic resistance of the wires is not included in the measurement. However, four-point measurements are inherently difficult due to the current path problem and non-ideal contacts between the electrode and the tissue sample, also known as the contact impedance, especially in tissue measurements. There are inherent difficulties in measuring the impedance of non-homogeneous materials [38].

One of the biggest challenges is the current path problem. This is the path taken by the current between the two injection electrodes, the current will follow the path of least resistance rather than the direct path predicted for a homogeneous material. While a four-point measurement configuration is preferred because of its ability to minimize contact impedance and parasitics, the current path problem is worse in a four-point measurement. The measurement of impedance using a collinear arrangement of four electrodes relies on the key assumption that the current driven between the outer pair of electrodes passes through the material uniformly, and thus the

voltage measured by the inner measurement electrodes can be used to calculate impedance from Ohm's law. If the current takes an unknown path between the injection electrodes instead of passing straight through the material below the measurement electrodes, the actual voltage generated within the material will be very small and the measured impedance will be erroneously low. In high precision measurement devices that use a range function to ensure linearity, the problem becomes worse. To maintain a constant voltage at the measurement electrodes with uncertainty about the current path results in an overloading of the drive circuitry and the inability to properly measure impedance.

The adjacent method (also known as the neighbouring method or the Sheffield data collection protocol) is applied in the measurements of this work [39]. In this method, the current is injected in two neighbouring electrodes and the voltage is measured from other successive adjacent electrode pairs. More concrete, in the first cycle of measurements, the current is injected in E1-E2 and the voltage is measured from the electrode pairs E2-E3, E3-E4, E4-E5, E5-E6, E6-E7, E7-E8, E8-E1. Note that electrode-pair E1-E2 was excluded from voltage measurements, but E2-E3 and E8-E1 were not. The next cycle of measurements is one with current injection on E2-E3 and voltage measurements from E3-E4, ..., E1-E2. After eight cycles of measurements, there are 56 voltage measurements available [40].

A lot of different methods for current injection and measuring patterns are described for electrical impedance tomography, but up till now, there is no consensus on what the ideal method is. In previous work, the adjacent method, the opposite method and the opposite driving/adjacent measuring method were compared to determine the best method for our setup and goal [36]. Based on visual interpretation, the adjacent method performed the most consistent and thus is the method of choice. Of course, the choice for this method implied a couple of benefits. Implementation of a minimal amount of hardware is one of the major benefits together with the high temporal resolution, compared to other methods. However, a downside is the current-density in the centre of the object under test. Because the excitation signals are between neighbouring electrodes, electrical field lines will remain close to the boundary. This means that the adjacent method is prone to noise and error [41]. As a noise reduction method, the Laplace prior opts as the most optimal way to determine the regularisation term (λ). The approach of this common edge-sensitive filter makes it possible to detect edges and to make the reconstruction of the phantom more demarcated [42].

The above measurement methodology is realized using a MUSEIC V2.0, a low power sensor with multiplexing capabilities developed by IMEC, Belgium [43]. The EIT image reconstruction made with the framework of EIDORS which is used in MATLAB 2018b, a compilation of algorithms that falls under the GNU Public License [44]. The duration of measuring all the potential values and the switching of the multiplexer takes in total 56.0s, for switching between the channels it takes 0.5s and again another 0.5s for the measurement itself. An electrical current of 100µA and a frequency of 10kHz was applied for the experiments.

2.6 Other Characterisations

Electrode to skin contact impedance is measured with medical electrodes (3M red dot electrodes) and the textile sensor. Two medical electrodes are attached to the skin, maintaining a definite spacing (2.5cm) between them. An electrical current of 100µA over a frequency range of 100Hz to 100kHz is applied between two electrodes and the corresponding voltage is measured between those electrodes to calculate the contact impedance. The measurements are repeated with textile electrodes attached to the skin surface, keeping the inter-electrode spacing the same as before.
The sensor strain measurements were established with the help of an inhouse made strain test bench. Both ends of the textile sensor were placed and attached firmly in between two metal plates. These holding plates move apart with a speed of 1cm/ minute, driving the stretching of the test specimen. Simultaneously, the electrode is connected to a multimeter through a Labview program to measure the corresponding resistance change due to stretching. The sheet resistance of the electrodes is measured with an in-house built Van der Pauw four-probe measurement system. The cross-sectional images of the printed sensor are made with Scanning Electron Microscopy (SEM). The SEM imaging is carried out with a FEI Quanta 200F electron microscopy, Hillsboro, USA)

3. Results and Discussion

3.1 EIT imaging for the human arm

To perform wearable EIT measurements, an arm wearable sensor band was designed and developed (sensor fabrication mentioned in section 2.2). As an initial step, a feasibility study was made on the wearable sensors for EIT imaging.

3.1.1 Printed flexible EIT sensor (non-stretchable) on textiles for forearm

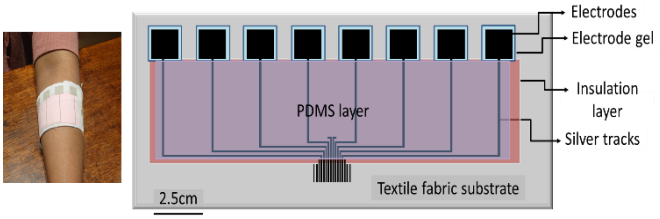

Fig4. The textile sensor is worn on the forearm (left), the design of the fabricated bioimpedance sensor (right).

As can be seen in Fig.4, the design of the sensor consists of 8 electrodes which were placed at equal distances over a length of 20cm. Each electrode has a dimension of 15mm by 15mm where the area of the electrode is inversely dependent on the contact impedance [45]. The electrodes were printed on the fabric without a planarizing layer and their sheet resistance is measured (four prob van der paw method) in the range of 0.065 to 0.1Ω/□. These electrodes were connected to the EIT measurement setup [36] through printed conductive tracks. An insulation layer was printed on top of the tracks to reduce the noise distortions in the EIT image. Further, an extra layer of PDMS was deposited to enhance the insulation functionality and to get an improved conformability and wearability of the device. The conductive electrode gel was applied onto the electrode structures using stencil printing to improve the signal to noise ratio by reducing the contact impedance. Fig.5 shows the SEM image of the cross-section of the sensor built-up.

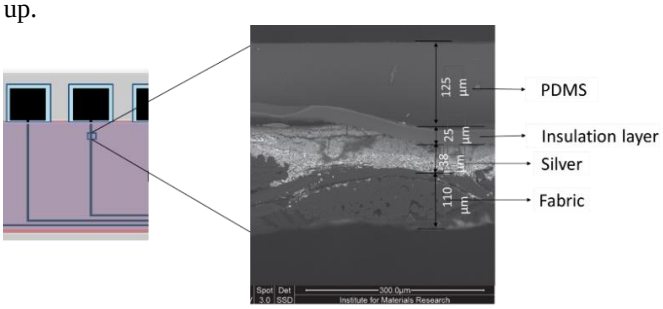

F*ig.5 SEM cross-sectional image of the sensor showing the built-up of the sensor using different printed layers.*

The bioimpedance sensor was tested on the human forearm (position shown in Fig. 6A) to obtain a 2D image of its cross-section. The non-stretchable flexible textile sensor is wrapped around the forearm and a little pressure is applied to bring the electrodes to adequate contact with the skin. The 2D image of the forearm cross-section created with the fabricated device is shown in Fig.6D.

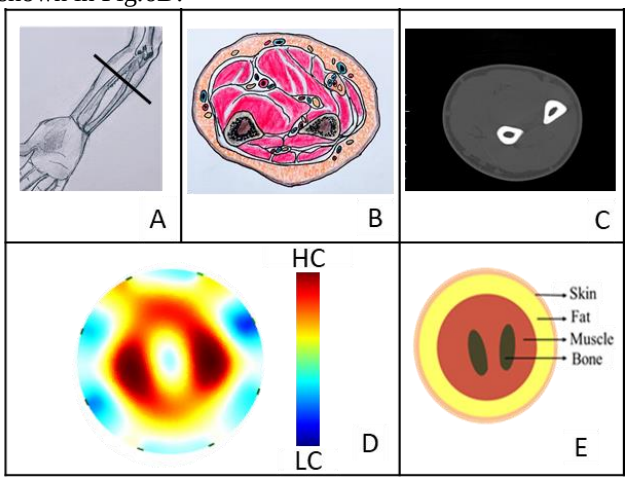

Fig.6 Human arm cross-section. Schematic picture of the position of the sensor (A), an anatomical cross-sectional pictorial of the forearm (B), the CT scan image of the forearm (C), EIT image reproduced with a printed sensor on textiles, HC: high conductive region, LC: low conductive region (D), Human arm cross-section simplified model [46, 47](E)

The bioimpedance measurements of the forearm cross-section obtained with the printed sensor produced an excellent EIT image (Fig.6D) comparable to the anatomical drawings in the literature (Fig.6B and 6E). The CT scan (Fig.6C) is a high-resolution forearm image where the bones' boundaries are clearly defined. Although the feature definition is less, the EIT image could also reproduce the bones' shape, size, and position, leading to some appealing possibilities. In the case of fracture dressing for patients, a sensor like the one described here could be easily printed on to it. Such a simple sensor is supposed to be sensitive to impedance changes that occur during the bone fracture healing stages and it could give real-time imaging info about healing [48-50]. A contrast in the electrical impedance of bone, muscle and fat tissue has been shown experimentally, and these spectral differences which EIT attempts to exploit and reproduces the forearm cross-section (bone 17583Ωcm, muscle 211Ωcm and fat 3850Ωcm [51]).

3.1.2 Printed sensor in reference to Ag/ AgCl medical electrodes (ECG patches)

Conventionally, hospitals use Ag/AgCl medical electrodes as a prior choice for biopotential measurements. The placement of eight or sixteen individual medical electrodes is a time consuming and labour intensive effort and removing them from the body causes pain [52]. The replacement of these electrodes with flexible textile sensors possesses a lot of medical perspectives. Alternative to medical electrodes, soft interfaced textile sensors enhance user convenience and reduce the preparation time for initiating a measurement. Apart from this, the textile sensors are fortunate not to have the bottleneck of EIT imaging using medical electrodes where the equidistant placement of the electrodes is a mandatory requirement for precise measurements [52, 53]. As the proof of functionality, the printed sensor tested in the EIT imaging is compared against the medical electrodes and shown in Fig. 7 A and B. Although there are some differences between the two images, the impedance mapping is essentially identical, proving the printed sensor's functionality. The root cause for the observed differences can be assigned to the contact impedance between the skin and the electrodes of the respective sensors [54]. The resultant graph in figure 7c indicates that the lesser contact impedance between the printed sensor and the skin contributes to better EIT images. Boone and Holder showed the contact impedance impact on the EIT image depiction in their work [55]. However, such contact impedance induced variations in the EIT imaging can be minimised with the right selection of frequency for the measurement.

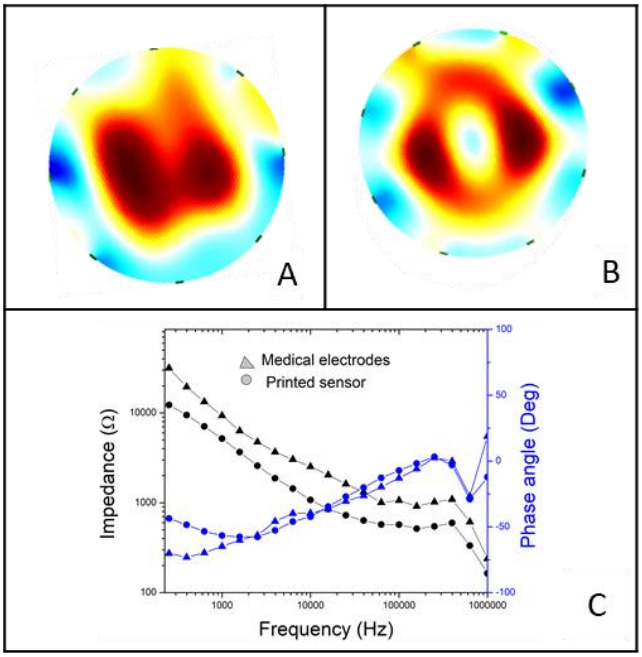

Fig.7 EIT images of human arm reproduced with medical electrodes (A) and printed textile sensor (B). Contact impedance measurement for the printed sensor and medical electrodes to skin shown in (C)

3.1.3 Influence of frequency on EIT imaging

The bioimpedance measurements are based on the electrical 'signature' nature of the biological tissues. The dependency of the electrical signal on the permeability of the different tissues produces distinct details in the images. The overall AC conductivity of the tissues can be summarised as [19]

$$\sigma = \sigma_0 + 2\pi f \varepsilon_0 \varepsilon'' \qquad \text{Eq.3}$$

Where σ_0 is the ionic conductivity of tissue, f is the frequency of measurements, ε_0 permittivity in space and ε'' is the imaginary component of tissue permittivity. Eq.3 shows how tissue conductivity varies with its composition and frequency. The founding father of biomedical engineering, H.P Schawn identified three different dispersions, i.e. changes in dielectric constants to the frequency in tissues occur in three different steps, namely alpha, beta and gamma dispersions [56]. This put forward the reliance of EIT imaging on frequency for different kind of tissues. For this reason, the bioimpedance measurements over a range of frequencies are more efficient compared to the measurements at a single frequency [22, 57]. However, EIT generally uses single frequency measurements, as multifrequency measurements have shown limited success. They often encounter systematic and sensitivity errors in impedance mapping (variability between measurements can lead to spatial inconsistencies) [58, 59]. In this work, the measurements were performed at three different frequencies to perceive its impact on image reproduction, as is shown in Fig.8. All three images depict the bones differently from one another in shape and size. This could be explained based on tissue properties and penetration depth dependency on the frequency of the signal. The frequency selection of the signals in most of the current EIT measurement systems is narrowed down to between 1 kHz and 2 MHz.

Another vital aspect to be considered is the contact impedance between electrode and skin. The skin is a multilayer organ in which the outer one is the stratum corneum made up of dead cells. This dead layer forms a barrier for biopotential signal, leading to contact impedance between electrode and skin [60]. The skin properties show considerable regional variability over the human body and contact impedance as well. A low-frequency measurement may suffer from high contact impedance between the skin and the electrodes which are shown in Fig.7C. Meanwhile, the high frequency could lead to enhanced parasitic capacitance associated with electrode circuitries introducing some measurement errors [21]. All these hints that selecting the right frequency is vital to obtain the body part's actual image. However, the appropriate frequency is dependent on different factors like the type of tissue, contact impedance and electrode spacing [21, 61, 62]. Although (as seen in Fig.8) the EIT image produced at a frequency of 10kHz seems to be the one with better features, it could be different in other measuring conditions. For instance, this experiment used dry electrodes instead of electrode gel; the resulting change in contact impedance leads to a higher frequency selection. Similarly, the frequency choice for bone fracture detection will be different from the instance of wound imaging due to the difference in tissue properties. Therefore, it can be concluded that the frequency selection is very subjective in nature and needs fine-tuning for each application to obtain an optimum image definition.

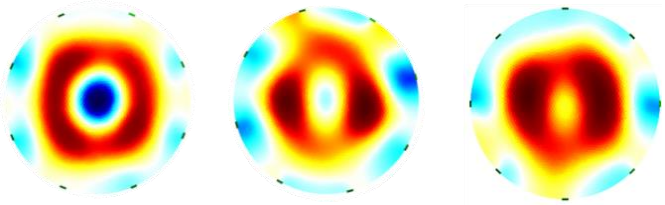

Fig.8 EIT images of the same arm cross-section at three different frequencies, 1 kHz (left), 10 kHz (middle), 100 kHz (right).

3.2 EIT imaging of the human thorax

This section deals with the human thorax imaging with a printed wearable stretchable textile sensor (sensor fabrication mentioned in section 2.3).

3.2.1 EIT imaging for thorax with the printed stretchable sensor

Due to the regular shape and the nearly static volume of the forearm, previous section experiment results showed no errors that arise from the bad contact of electrodes with the body part. However, for a body part like the thorax, having an uneven shape and a continuous volume change, more complexities are added to the EIT imaging. The thorax imaging with bioimpedance sensor faced difficulty obtaining homogeneous contact with the body due to its irregular topography and breathing, leading to measurement errors. To counteract these motion artefacts and inadequate contact, several precautions are taken in the work. To enhance the electrode thorax interface contact and to attain a simultaneous autotuning in the perimeter of the sensor along with breathing, the effort extended to the development of a stretchable sensor. During the course of thorax imaging, the sensor on the textile was stretched to 15-20% of its original dimension (perpendicular to the conductive track direction) and the resistance of the electrodes and the tracks had shown only minor change. The stretchability of the sensor is tested with the help of strain-resistance measurements. Fig.9 illustrates the change in resistance of conductive tracks of the sensor due to stretching and the change is about 5-10% of the initial resistance. However, the influence of this resistance change is negligible compared to the contact impedance of the electrode to the skin. The breathing phases of inhaling and exhaling exert different stretching to the sensor. It causes to induce different amounts of pressure on the electrode to the body. However, this varying pressure on electrodes does not significantly influence the contact impedance when there is an electrode gel in between [63]. Besides, the PDMS layer, which first of all serves as an insulation layer has a double purpose. It will also serve as a kind of anti-slip layer to prevent any movement of the stretchable sensor, relative to the skin of the subject, during a measurement.

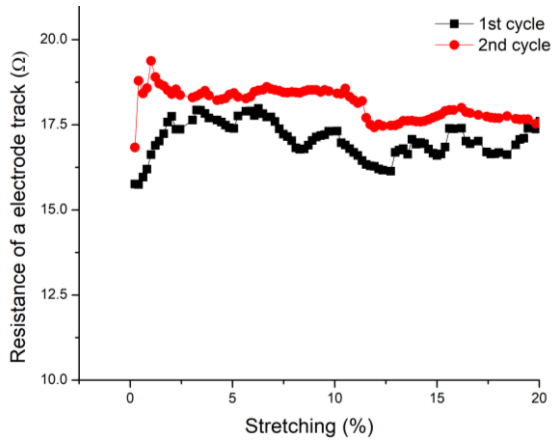

Fig.9 Resistance of the electrode tracks plotted against stretching

Measurements on the thorax were made with a 16 electrode stretchable sensor (the fabrication described in section 2.3)) and it is different from that for the forearm measurements. This difference in electrode arrangement is due to the contrast in the perimeter of the forearm and the thorax. The EIT image was created with the printed sensor worn on the thorax position (Fig.10A) and the impedance measurements were carried out by applying a current of 100 µA and a frequency of 10 kHz. The resultant EIT image, as shown in Fig.10C maps the conductivity distribution of the lungs and it lines up with the image (Fig.10B) and with the literature[64, 65]. Anyhow, some image artefacts occurred from the measurements and the dark blue shades in Fig.10C resulted from such measurement errors.

The EIT image reproduced with the printed sensor is proof of the working principle of a stretchable bioimpedance sensor on textile for EIT imaging of thorax. Medical imaging for monitoring the functioning of the lungs has a great significance. The lung is one of the largest organs in the human body and it has got a much higher resistivity as compared to other soft tissues. The rise in air volume causes the resistivity of the lungs to increase further. [66-68]. This makes EIT a notable technique to assess the breath functioning by monitoring the size and shape of the lungs in a real-time manner. Some studies prove the feasibility of the EIT technique to learn the regional ventilation of intensive care patient's lungs as an efficient method to guide the ventilator settings [52, 67, 69].

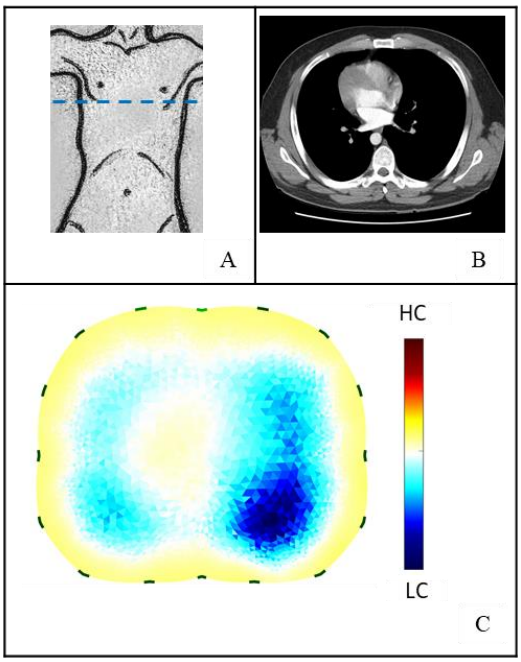

Fig.10 Thorax imaging, the position of the sensor worn (A), CT scan image (Case courtesy of Dr. Andrew Dixon, Radiopaedia.org, rID: 36676)(B), EIT imaging for thorax with the printed sensor on stretchable fabric (C)

3.2.2 Impact of the number of electrodes on EIT image quality

EIT measurement systems are inherently attributed to low-resolution images compared to other imaging modalities such as CT or MRI scans [21, 52]. The disadvantages of EIT imaging arise from different factors such as the relatively low resolution of the measurable data, troubling signal-to-noise ratio and the constrained algorithm [70]. One way to improve the resolution of the measured data is to increase the measurement count by expanding the number of electrodes [71]. The EIT image quality to the number of electrodes could be correlated in a comparable way as picture quality correlates to camera pixels [21]. However, the addition of electrodes is limited as it further increases the measurement complexity and the output data is more susceptible to interference and measurement errors [71]. Besides, adding more electrodes implies longer measurement times and reduces the temporal resolution of the system. Another factor that needs to be taken into account, when increasing the number of electrodes, is the necessity of more complex hardware and an increase in computation costs as the reconstruction algorithm needs to handle larger datasets. Nevertheless, within the possible window, measurements were conducted to see the influence of the number of electrodes in rendering the quality of the image. Fig.11 represents the EIT imaging of the thorax for an 8 and 16 electrode configuration. It exhibited an enhancement in the definition of the lung outline on increasing the number of electrodes from 8 to 16. The image made with the 8 electrode arrangement suffered from a lower resolution, blurred details and inaccurate boundary mapping whereas the latter reproduces the lung's position, size and shape with better quality (light blue colour indicates the lungs).

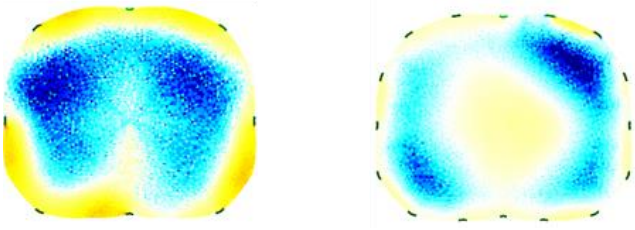

Fig.11 EIT images for thorax with 8 electrodes (left), 16 electrodes (right). (The short marks on the periphery indicates the position of the electrodes in the measurements)

4. Conclusion and outlook

Wearable bioimpedance sensors for EIT imaging printed on both stretchable and non-stretchable textiles were demonstrated as a conceivable method for health assessment of the human body. Industrially applicable and roll-to-roll compatible processes were deployed for the fabrication of sensors. The investigation achieves these objectives and the fabricated sensor was applied to render tomographic 2D images of human body parts. The EIT imaging on the forearm generated different colour shades for bones and the tissues surrounding the bones based on the conductivity distribution. The functionality of the sensor was cross-checked with a conventional sensor (ECG patches) used for EIT imaging as well as compared to CT images. The impact of the number of electrodes in rendering quality images was evident from the features of the image. The frequency response of the tissue and the impact of signal frequency in image rendering quality is shown in the results. Likewise, the applicability of a stretchable bioimpedance sensor for lung imaging is proven to be a potential tool. Hence the functionality of fully printed wearable impedance sensors is verified as a possible method for portable applications of scanning and the influence of important parameters such as frequency and the number of electrodes, on imaging are studied and explained.

Compared to the conventional EIT measurement systems, configuring the measurement setup for a printed bioimpedance sensor consumes only a little time and provides high accuracy in measurements due to lower contact impedance and the placement of electrodes at equal distances [3]. Wearable and compact impedance analysers for EIT imaging were reported in different works and are commercialized [28, 72-74]. Having these compact impedance analysers integrated with printed textile sensors introduces the possibilities of wearable, low cost and radiation-free continuous health monitoring modalities. Recent studies have shown that the impedance of the wound increases gradually over time on healing. Real-time monitoring of the wound healing with a printed sensor on the wound dressing integrated with a mobile impedance analyser can help better understand the wound healing process and eventually help wound diagnosis.

Acknowledgements

The authors would like to acknowledge Prof. Jan D'Haen from Hasselt University for providing SEM images.

References

[1] S. P. Sreenilayam, I. U. Ahad, V. Nicolosi, V. Acinas Garzon, and D. Brabazon, "Advanced materials of printed wearables for physiological parameter monitoring," *Materials Today*, 2019.

[2] M. Pooria, N. A. Sanati, M. Nikkhah, and M. Akbari, "Flexible Electronic Devices for Biomedical Applications," in *Advanced Mechatronics and MEMS Devices II*: Springer Cham, 2017, pp. 341-366.

[3] S. Majumder, T. Mondal, and M. J. Deen, "Wearable Sensors for Remote Health Monitoring," (in eng), *Sensors*, vol. 17, no. 1, p. 130, Jan. 2017.

[4] M. Ochoa, R. Rahimi, and B. Ziaie, "Flexible sensors for chronic wound management"," *Biomed Eng, IEEE Rev*, vol. 7, 2014.

[5] Kenry, J. C. Yeo, and C. T. Lim, "Emerging flexible and wearable physical sensing platforms for healthcare and

biomedical applications," *Microsyst Nanoeng*, Review Article vol. 2, no. 1, p. 16043, Dec. 2016.

[6] L. Castano and A. Flatau, "Smart fabric sensors and e-textile technologies: A review," *Smart Mater. Struct.* , vol. 23, no. 5, p. 053001, May. 2014.

[7] M. Stoppa and A. Chiolerio, "Wearable electronics and smart textiles: a critical review," (in eng), *Sensors (Basel, Switzerland)*, vol. 14, no. 7, pp. 11957-11992, 2014.

[8] R. Paradiso, G. Loriga, and N. Taccini, "A wearable health care system based on knitted integrated sensors," *IEEE Trans. Inf. Techn. Biomed.*, vol. 9, no. 3, pp. 337-344, Sep. 2005.

[9] T. Carey *et al.*, "Fully inkjet-printed two-dimensional material field-effect heterojunctions for wearable and textile electronics," *Nat Commun*, vol. 8, no. 1, p. 1202, Dec. 2017.

[10] J. Liu, Y. Li, S. Yong, S. Arumugam, and S. Beeby, "Flexible Printed Monolithic-Structured Solid-State Dye Sensitized Solar Cells on Woven Glass Fibre Textile for Wearable Energy Harvesting Applications," *Scientific Reports*, vol. 9, no. 1, p. 1362, 2019/02/04 2019.

[11] T. Blecha, R. Linhart, and J. Reboun, "Screen printed antennas on textile substrate," in *5th Electronics System-integration Technology Conference*, Helsinki, 2014, pp. 1-4: IEEE.

[12] T.-h. Huang *et al.*, "A Novel Design of E-Textile Integration for Physiological Monitoring and Lighting," *J. Fashion. Technol. Textile. Eng*, vol. 0, no. 4, Feb. 2018 2018.

[13] W. Urbaniak-Domagala, E. Skrzetuska, M. Komorowska, and I. Krucińska, "Development Trends in Electronics Printed: Intelligent Textiles Produced with the Use of Printing Techniques on Textile Substrates," in *Printed Electronics: Current Trends and Applications*, I. Yun, Ed. Rijeka: InTechOpen, 2016

[14] I. Verboven, J. Stryckers, V. Mecnika, G. Vandevenne, M. Jose, and W. Deferme, "Printing Smart Designs of Light Emitting Devices with Maintained Textile Properties," *Materials*, vol. 11, no. 2, p. 290, Feb. 2018.

[15] J. Suikkola *et al.*, "Screen-Printing Fabrication and Characterization of Stretchable Electronics," *Sci Rep*, vol. 6, p. 25784, May. 2016.

[16] P. Gordon, "Screen printed textile based wearable biopotential monitoring," PhD dissertation, Physical Sciences and Engineering, University of Southampton, Southampton, 2014.

[17] S. Hong *et al.*, "A 4.9 mΩ-Sensitivity Mobile Electrical Impedance Tomography IC for Early Breast-Cancer Detection System," *IEEE Journal of Solid-State Circuits*, vol. 50, no. 1, pp. 245-257, 2015.

[18] S. L. Swisher *et al.*, "Impedance sensing device enables early detection of pressure ulcers in vivo," *Nat Commun*, Article vol. 6, p. 6575, May. 2015.

[19] R. Pethig, "Dielectric properties of body tissues," *Clinical Physics and Physiological Measurement*, vol. 8, no. 4A, pp. 5-12, 1987/11 1987.

[20] S. Khalil, M. Mohktar, and F. Ibrahim, "The Theory and Fundamentals of Bioimpedance Analysis in Clinical Status Monitoring and Diagnosis of Diseases," *Sensors*, vol. 14, no. 6, p. 10895, Jun. 2014.

[21] B. H. Brown, "Electrical impedance tomography (EIT): a review," *J. Med. Eng. Tech.*, vol. 27, no. 3, pp. 97-108, Jun. 2003.

[22] T. K. Bera, "Bioelectrical Impedance Methods for Noninvasive Health Monitoring: A Review," *J. Med. Eng. Technol.*, p. 28, Jun. 2014.

[23] M. A. Thomasset, "[Bioelectric properties of tissue. Impedance measurement in clinical medicine. Significance of curves obtained]," (in fre), *Lyon Med*, vol. 94, pp. 107-18, Jul 15 1962.

[24] R. Bayford and A. Tizzard, "Bioimpedance imaging: an overview of potential clinical applications," *Analyst*, vol. 137, no. 20, pp. 4635-4643, Oct. 2012.

[25] S. Khalil, M. Mohktar, and F. Ibrahim, "The Theory and Fundamentals of Bioimpedance Analysis in Clinical Status Monitoring and Diagnosis of Diseases," *Sensors*, vol. 14, no. 6, p. 10895, 2014.

[26] J. H. Park, Y.-I. Jo, and J.-H. Lee, "Clinical usefulness of bioimpedance analysis for assessing volume status in patients receiving maintenance dialysis," (in eng), *The Korean journal of internal medicine*, vol. 33, no. 4, pp. 660-669, 2018.

[27] C. Earthman, D. Traughber, J. Dobratz, and W. Howell, "Bioimpedance spectroscopy for clinical assessment of fluid distribution and body cell mass," (in eng), *Nutr Clin Pract*, vol. 22, no. 4, pp. 389-405, Aug 2007.

[28] S. Hong, J. Lee, and H. Yoo, "Wearable lung-health monitoring system with electrical impedance tomography," in *37th Annual International Conference of the IEEE Engineering in Medicine and Biology Society* Milan, 2015, pp. 1707-1710: IEEE.

[29] H. Li, R. Chen, C. Xu, B. Liu, X. Dong, and F. Fu, "Combing signal processing methods with algorithm priori information to produce synergetic improvements on continuous imaging of brain electrical impedance tomography," *Sci. Rep.*, vol. 8, no. 1, p. 10086, Dec. 2018.

[30] E. Teschner, M. Imhoff, and S. Leonhardt, *Electrical Impedance Tomography: The realisation of regional ventilation Monitoring, 2nd edition*. 2015.

[31] Y. Zhang and C. Harrison, "Tomo: Wearable, Low-Cost Electrical Impedance Tomography for Hand Gesture Recognition," in *28th Annual ACM Symposium on User Interface Software Technology*, Charlotte, pp. 167-173: ACM.

[32] A. Chanda, "Biomechanical Modeling of Human Skin Tissue Surrogates," *Biomimetics*, vol. 3, no. 3, p. 18, 2018.

[33] D. Gregor-Svetec, "Chapter 8 - Intelligent Packaging," in *Nanomaterials for Food Packaging*, M. Â. P. R. Cerqueira, J. M. Lagaron, L. M. Pastrana Castro, and A. A. M. de Oliveira Soares Vicente, Eds.: Elsevier, 2018, pp. 203-247.

[34] H. Kipphan, *Handbook of Print Media: Technologies and Production Methods*. Springer-Verlag New York, Inc., 2006.

[35] R. Torah, Y. Wei, Y. Li, K. Yang, S. Beeby, and J. Tudor, "Printed Textile-Based Electronic Devices," 2015.

[36] M. Lemmens, H. Biesmans, S. Bormans, T. Vandenryt, and R. Thoelen, "Electrical Impedance Tomography With a Lab-on-Chip for Imaging Cells in Culture," *Phys. Status Solidi A*, vol. 215, no. 15, p. 1700868, Aug. 2018.

[37] D. Holder, *Electrical Impedance Tomography: Methods, History and Applications*. CRC Press, 2004.

[38] S. L. Swisher *et al.*, "Impedance sensing device enables early detection of pressure ulcers in vivo," *Nature Communications*, vol. 6, no. 1, p. 6575, 2015/03/17 2015.

[39] B. H. Brown, Seagar, A. D., "The Sheffield data collection system," *Clin. Phys. Physiol. Meas.*, vol. 8, no. suppl. A, 1987.

[40] T. K. Bera and J. Nagaraju, "Studying the resistivity imaging of chicken tissue phantoms with different current patterns in Electrical Impedance Tomography (EIT)," *Measurement*, vol. 45, no. 4, pp. 663-682, 2012/05/01/ 2012.

[41] W. R. Breckon and M. K. Pidcock, "Mathematical aspects of impedance imaging," (in eng), *Clin. Phys. Physiol. Meas.*, vol. 8 Suppl A, pp. 77-84, 1987.

[42] U. Pliquett *et al.*, "Testing miniaturized electrodes for impedance measurements within the β-dispersion – a practical approach," (in English), *Journal of Electrical Bioimpedance*, vol. 1, no. 1, p. 41, 01 Jan. 2010 2010.

[43] H. Ha *et al.*, "A bio-impedance readout IC with frequency sweeping from 1k-to-1MHz for electrical impedance tomography," in *2017 Symposium on VLSI Circuits*, 2017, pp. C174-C175.

[44] A. Adler and W. R. B. Lionheart, "Uses and abuses of EIDORS: an extensible software base for EIT," *Physiological Measurement*, vol. 27, no. 5, pp. S25-S42, 2006/04/18 2006.

[45] M. H. Jung *et al.*, "Wrist-wearable bioelectrical impedance analyzer with contact resistance compensation function," in *IEEE SENSORS*, Orlando, 2016, pp. 1-3: IEEE.

[46] K. Ito and Y. Hotta, "Signal Path Loss Simulation of Human Arm for Galvanic Coupling Intra-body Communication," presented at the IEEE Twelfth International Symposium on Autonomous Decentralized Systems, Taichung Aug. 2016,

[47] B. Mochnacki and M. Ciesielski, "Sensitivity of transient temperature field in domain of forearm insulated by protective clothing with respect to perturbations of external boundary heat flux," (in English), *Numer Heat Tr A-Appl*, vol. 64, no. 3, p. 591, Sep. 2016.

[48] A. H. Dell'Osa, "Bone Electrical Impedance and Tomographic Reconstruction of Fracture Detection: A Review," in *II Latin American Conference on Bioimpedance*, Singapore, 2016, vol. 54, pp. 12-15: Springer Singapore.

[49] M. C. Lin, D. Hu, M. Marmor, S. T. Herfat, C. S. Bahney, and M. M. Maharbiz, "Smart bone plates can monitor fracture healing," *Scientific Reports*, vol. 9, no. 1, p. 2122, 2019/02/14 2019.

[50] H. C. N. Jongschaap, R. Wytch, J. M. S. Hutchison, and V. Kulkarni, "Electrical impedance tomography: a review of current literature," *European Journal of Radiology*, vol. 18, no. 3, pp. 165-174, 1994/08/01/ 1994.

[51] T. J. C. Faes, H. A. van der Meij, J. De Munck, and R. M. Heethaar, "The electric resistivity of human tissues (100 HZ-10 MHZ): A meta- analysis of review studies," *Physiol. Meas.*, vol. 20, no. 4, pp. R1-10, Dec. 1999.

[52] E. Teschner, M. Imhoff, and S. Leonhardt, "Electrical Impedance Tomography: The realisation of regional ventilation monitoring 2nd edition," D. A. C. KGaA, Ed., ed. Lübeck: Dräger Medical GmbH, 2015, p. 147.

[53] T. Ouypornkochagorn, "Influence of Electrode Placement Error and Contact Impedance Error to Scalp Voltage in Electrical Impedance Tomography Application," in *2019 7th International Electrical Engineering Congress (iEECON)*, 2019, pp. 1-4.

[54] V. Kolehmainen, M. Vauhkonen, P. A. Karjalainen, and J. P. Kaipio, "Assessment of errors in static electrical impedance tomography with adjacent and trigonometric current patterns," *Physiol. Meas.*, vol. 18, no. 4, pp. 289-303, Nov. 1997.

[55] K. G. Boone and D. S. Holder, "Effect of skin impedance on image quality and variability in electrical impedance tomography: a model study," *Medical and Biological Engineering and Computing*, vol. 34, no. 5, pp. 351-354, 1996/09/01 1996.

[56] H. P. Schwan, "Electrical properties of tissues and cell suspensions: mechanisms and models," in *Proceedings of 16th Annual International Conference of the IEEE Engineering in Medicine and Biology Society*, 1994, vol. 1, pp. A70-A71 vol.1.

[57] J. P. Langlois, Y. Wu, R. Bayford, and A. Demosthenous, "On the application of frequency selective common mode feedback for multifrequency EIT," *Physiol. Meas.*, vol. 36, no. 6, p. 1337, Jun. 2015.

[58] N. Goren *et al.*, "Multi-frequency electrical impedance tomography and neuroimaging data in stroke patients," *Sci Data*, Data Descriptor vol. 5, p. 180112, Jul. 2018.

[59] J. Avery, T. Dowrick, M. Faulkner, N. Goren, and D. Holder, "A Versatile and Reproducible Multi-Frequency Electrical Impedance Tomography System," *Sensors (Basel, Switzerland)*, vol. 17, 2017.

[60] A. Albulbul, "Evaluating Major Electrode Types for Idle Biological Signal Measurements for Modern Medical Technology," (in eng), *Bioengineering (Basel, Switzerland)*, vol. 3, no. 3, p. 20, 2016.

[61] A. Boyle and A. Adler, "The impact of electrode area, contact impedance and boundary shape on EIT images," *Physiological measurement*, vol. 32, pp. 745-54, 07/01 2011.

[62] E. Malone, G. S. d. Santos, D. Holder, and S. Arridge, "Multifrequency Electrical Impedance Tomography Using Spectral Constraints," *IEEE Trans Med Imaging*, vol. 33, no. 2, pp. 340-350, Feb. 2014.

[63] R. Kusche, S. Kaufmann, and M. Ryschka, "Dry electrodes for bioimpedance measurements—design, characterization and comparison," *Biomedical Physics & Engineering Express*, vol. 5, no. 1, p. 015001, 2018/11/08 2018.

[64] H. H. Aung, A. Sivakumar, S. K. Gholami, S. P. Venkateswaran, B. Gorain, and Shadab, "Chapter 1 - An Overview of the Anatomy and Physiology of the Lung," in *Nanotechnology-Based Targeted Drug Delivery Systems for Lung Cancer*, P. Kesharwani, Ed.: Academic Press, 2019, pp. 1-20.

[65] D. Bell and J. Jones. Anatomy: Thoracic [Online]. Available: https://radiopaedia.org/?lang=us

[66] I. Chatziioannidis, T. Samaras, and N. Nikolaidis, "Electrical Impedance Tomography: a new study method for neonatal Respiratory Distress Syndrome," *Hippokratia*, vol. 15, no. 3, pp. 211-215, Jul. 2011.

[67] J. Riera, P. J. Riu, P. Casan, and J. R. Masclans, "Tomografía de impedancia eléctrica en la lesión pulmonar aguda," *Medicina Intensiva (English Edition)*, vol. 35, no. 8, pp. 509-517, Nov. 2011.

[68] J. Zhang and R. Patterson, "Variability in EIT Images of Lung Ventilation as a Function of Electrode Planes and Body Positions," *TOBEJ*, vol. 8, no. 1, pp. 35-41, Jun. 2014.

[69] J. C. Richard *et al.*, "Electrical impedance tomography compared to positron emission tomography for the measurement of regional lung ventilation: an experimental study," *Crit. Care*, vol. 13, no. 3, p. R82, May. 2009.

[70] V. Chitturi and F. Nagi, "Spatial resolution in electrical impedance tomography: A topical review," *J. Electr. Bioimped.*, Array processing; Current patterns; Data acquisition; Direct algorithms; EIT hardware; Electrodes; Fusion techniques; Iterative algorithm vol. 8, no. 1, pp. 66-78, Apr. 2017.

[71] M. Tang, W. Wang, J. Wheeler, M. McCormick, and X. Dong, "The number of electrodes and basis functions in EIT image reconstruction," (in eng), *Physiol. Meas.*, vol. 23, no. 1, pp. 129-40, Feb. 2002.

[72] C. Gibas, A. Grünewald, S. Büchner, and R. Brück, "An EIT system for mobile medical diagnostics," in *SPIE Medical Imaging*, Houston, 2018, vol. 10578, p. 9: SPIE.

[73] S. Lee *et al.*, "A Low-power and Compact-sized Wearable Bio-impedance Monitor with Wireless Connectivity," *J. Phys.: Conf. Ser.*, vol. 434, no. 1, p. 4, Apr. 2013.

[74] IMEC. *Biomedical sensor systems-on-chip*. Available: https://www.imec-int.com/en/system-on-chip